Title

A Bifunctional Ionic Liquid for Capture and Electrochemical Conversion of CO2 to CO over Silver

Journal

ACS Catalysis, 13(12)

ISSN

2155-5435

Authors

Dongare, Saudagar

Coskun, Oguz Kagan

Cagli, Eda

et al.

Publication Date

2023-06-16

DOI

10.1021/acscatal.3c01538

Peer reviewed

ACS Catalysis

pubs.acs.org/acscatalysis

Research Article

A Bifunctional Ionic Liquid for Capture and Electrochemical Conversion of CO_2 to CO over Silver

Saudagar Dongare, Oguz Kagan Coskun, Eda Cagli, Kevin Y. C. Lee, Guodong Rao, R. David Britt, Louise A. Berben, and Burcu Gurkan*

Cite This: *ACS Catal.* 2023, 13, 7812–7821

Read Online

ACCESS | Metrics & More | Article Recommendations | Supporting Information

ABSTRACT: Electrochemical conversion of CO_2 requires selective catalysts and high solubility of CO_2 in the electrolyte to reduce the energy requirement and increase the current efficiency. In this study, the CO_2 reduction reaction (CO_2RR) over Ag electrodes in acetonitrile-based electrolytes containing 0.1 M [EMIM][2-CNpyr] (1-ethyl-3-methylimidazolium 2-cyanopyrolide), a reactive ionic liquid (IL), is shown to selectively (>94%) convert CO_2 to CO with a stable current density (6 mA·cm^{-2}) for at least 12 h. The linear sweep voltammetry experiments show the onset potential of CO_2 reduction in acetonitrile shifts positively by 240 mV when [EMIM][2-CNpyr] is added. This is attributed to the pre-activation of CO_2 through the carboxylate formation via the carbene intermediate of the $[EMIM]^+$ cation and the carbamate formation via binding to the nucleophilic $[2\text{-CNpyr}]^-$ anion. The analysis of the electrode−electrolyte interface by surface-enhanced Raman spectroscopy (SERS) confirms the catalytic role of the functionalized IL where the accumulation of the IL-CO_2 adduct between −1.7 and −2.3 V vs Ag/Ag$^+$ and the simultaneous CO formation are captured. This study reveals the electrode surface species and the role of the functionalized ions in lowering the energy requirement of CO_2RR for the design of multifunctional electrolytes for the integrated capture and conversion.

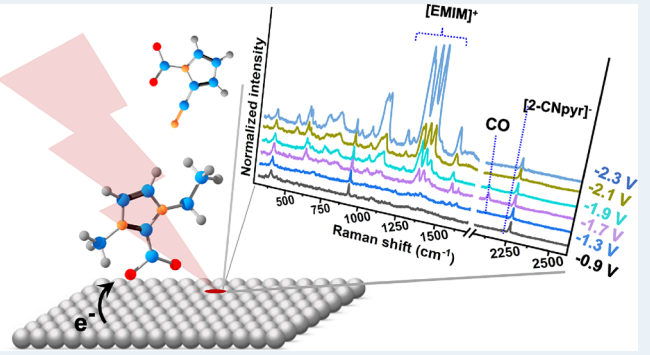

KEYWORDS: *electrochemical CO_2 reduction, ionic liquid, faradaic efficiency, carbon monoxide, carbon capture and utilization*

INTRODUCTION

The CO_2 concentration in the atmosphere is rapidly increasing due to anthropogenic activities. As a result, the average global atmospheric temperature is increasing, causing a rise in sea levels and ocean acidification.[1,2] Converting CO_2 into fuels or common chemicals offers hope for an energy transition from non-renewable to sustainable energy resources, which mitigates the adverse effects arising from increasing CO_2 in the atmosphere. The CO_2 conversion can be achieved by a variety of methods, including thermochemical,[3,4] biochemical,[5] photochemical,[6] electrochemical,[5] and radiochemical.[7] Among the available CO_2 conversion techniques, electrochemical CO_2 reduction reaction (CO_2RR) offers certain advantages: (1) mild operating conditions, (2) environmental compatibility (energy required to drive CO_2RR can be derived from renewable energy resources like solar and wind), (3) easy control of product selectivity by adjusting external parameters such as electrolytes and applied voltages, and (4) engineering and economic feasibility.[8,9] Significant efforts have been devoted in developing metal[10] and non-metal catalysts,[11] modifications to catalyst morphology and composition,[12] and electrolyzer configuration[13] for CO_2RR in aqueous electrolytes. However, several existing challenges such as low solubility of CO_2, the competing hydrogen evolution reaction, and instability of metal and metal oxide catalysts in (acid) aqueous environments need to be addressed to enhance the efficiency.[14]

Ionic liquids (ILs) have been considered for CO_2RR due to their high electrochemical stabilities, high CO_2 solubilities, negligible vapor pressures, and tunable physical properties.[15−18] It has been reported that ILs can activate thermodynamically stable CO_2 and accelerate its transfer to the reaction interface, acting as "co-catalysts".[19,20] One of the earlier studies was by Rosen et al.[19] where the reduction of CO_2 to CO on a Ag electrode utilizing 1-ethyl-3-methylimidazolium tetrafluoroborate ([EMIM][BF_4]) with 18 mol % water was achieved. They reported CO generation at a lower overpotential (difference between the thermodynamic and experimental reduction potentials) compared to aqueous systems and with stable performance for 7 h with

Received: April 4, 2023
Revised: May 9, 2023
Published: May 25, 2023

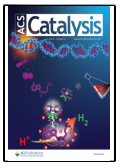

Faradaic efficiency of >96%. They attributed these improvements to the stabilization of the $CO_2^{\bullet-}$ intermediate by $[EMIM]^+$. Furthermore, Braunschweig's group[21−23] studied the role of imidazolium cations with the same $[BF_4]^-$ for CO_2 to CO conversion over Pt catalysts by operando IR absorption spectroscopy and in situ sum frequency generation spectroscopy. They reported the reduction of the imidazolium cation to carbene, which was discussed to subsequently react with CO_2 to form an imidazolium-2-carboxylic acid specie. This reactive intermediate underwent a proton-coupled electron transfer (500 mM water as the proton source), thus leading to CO formation and regeneration of the imidazolium cation. Hanc-Scherer et al.[15] and Zhao et al.[24] reported the formation of a stable EMIM-H-CO_2 adduct by a radical−radical coupling after the simultaneous reduction of CO_2 and $[EMIM]^+$. In these studies, the EMIM-H-CO_2^- adduct is discussed to form upon the reaction of radical species: $CO_2^{\bullet-}$ and $[EMIM]^\bullet$ (generated by single electron transfer to $[EMIM]^+$).

There are also few reports where the role of the IL anions was investigated.[25,26] Golru and Biddinger[25] showed the impact of anions' hydrophilicity, size, and CO_2 affinity on CO_2RR. They studied ILs with the 1-butyl-3-methylimidazolium ($[BMIM]^+$) cation and the following anions: (bis-(trifluoromethylsulfonyl)imide ($[TFSI]^-$), triflate ($[OTF]^-$), acetate ($[Ac]^-$), chloride ($[Cl]^-$), and dicyanamide ($[DCA]^-$). They used 10 mM of IL in 0.1 M $KHCO_3$ solution and examined CO_2RR on a electropolished copper surface. They found that formate is selectively generated at −0.92 V versus RHE (reference hydrogen electrode) with the exception of the electrolyte with $[DCA]^-$ where H_2 was the major product. In another study, Kang et al.[26] reported that ILs with fluorinated anions such as trifluoromethylsulfonate ($[OTf]^-$), hexafluorophosphate ($[PF_6]^-$), and tetrafluoroborate ($[BF_4]^-$) when paired with $[BMIM]^+$ enable conversion of CO_2 to CH_4 with higher total current densities compared to a non-fluorinated perchlorate anion ($[ClO_4]^-$) on Zn-based metal−organic frameworks (Zn−MOFs) as the solid catalyst. The increase in current density was explained to be due to (1) strong interactions between CO_2 and fluorine atoms on the anions and (2) the strong adsorption capacity of CO than CH_4 on the Zn-MOF.

In summary, the majority of the CO_2RR studies with ILs thus far have focused on common ILs where CO_2 is physisorbed in the absence of electric fields. Specifically, ILs with imidazolium cation are shown to lower the activation energy[19] by co-catalyzing the reaction at the metal electrode surface, suppressing hydrogen evolution reaction (HER),[27] and increasing CO_2 solubility[28,29] with control over the reaction pathway.[30] These studies suggest that surface adsorption of ILs plays an important role in lowering HER; however, the exact mechanism by which ILs lower the overpotential remains unclear. Both an inner sphere e-transfer[31] for surface-adsorbed CO_2 and a carboxylated imidazolium promoted route[19,20] have been discussed. In contrast to these studies, there has been a single report where a reactive IL, trihexyltetradecylphosphonium 1,2,4-triazole ($[P_{66614}][124Triz]$), that chemisorbs CO_2 was studied for CO_2RR.[29] It was reported that $[124Triz]^-$ chemisorbs CO_2 in equimolar quantity. The covalently bound CO_2 on $[124Triz]^-$ was discussed to be reduced on Ag at overpotentials as low as 0.17 V (vs Ag/Ag^+), generating formate as the major product. However, this study did not provide spectroscopic evidence to the surface species or the reaction mechanism.

Here, we examined the reactive IL [EMIM][2-CNpyr] in acetonitrile, where the chemisorption of CO_2 yields carboxylate and carbamate species as a result of CO_2 binding to $[EMIM]^+$ and $[2\text{-}CNpyr]^-$, respectively. Specifically, we studied the role of these species in modulating the CO_2RR mechanism on Ag by voltammetry and SERS studies with systematic variations in the molecular structure of the IL, thus probing the individual functionality. The role of the local electrolyte environment in the bulk and at the electrode−electrolyte interface is shown to have a critical role in lowering the reduction potentials and reaction efficiency and selectivity.

EXPERIMENTAL SECTION

Materials and Methods. 1-Ethyl-3-methyl-imidazolium chloride ([EMIM][Cl]) and 1-ethyl-3-methyl-imidazolium bis(trifluoromethylsulfonyl)imide ([EMIM][TFSI]) were purchased from IoLiTec Inc. Pyrrole 2-carbonitrile (99%) was from Thermo Scientific Chemicals and amberlite IRN-87 anion exchange resin (AER) were purchased from Purolite. Amberlite IRN-87 AER was washed multiple times with methanol and vacuum dried at room temperature to remove impurities present in it. Molecular sieves (3 Å) were received from Merck (Germany) and used after overnight drying at 100 °C under vacuum. 1,2-Dimethyl imidazole (98%) and bromo ethane (99%) were purchased from Alfa Aesar and TCI, respectively. Tetraethylammonium perchlorate (TEAP, 99.0%), choline chloride ([Ch][Cl], 99%), diethyl ether (>99%, anhydrous), and acetonitrile (99.9%) were obtained from Sigma-Aldrich. Methanol (99.8%, HPLC grade) and ethyl acetate (99.9%) were purchased from Fisher. A glass fiber nonwoven filter (Whatman grade GF/A, 260 μm in thickness) was purchased from VWR. Silver foil (99.9%) was obtained from Sigma-Aldrich. A Pt mesh electrode (99.9%, 4 cm^2 area) and a non-aqueous reference electrode kit-Ag/Ag^+ were purchased from BASi. For NMR characterizations, deuterated dimethyl sulfoxide-d6 (DMSO-d6, 99.9% (isotopic)) and chromium(III) acetylacetonate (99.99%) were purchased from Thermo Scientific and Sigma-Aldrich, respectively. High-purity N_2 (99.999%), Ar (99.999%), CO_2 (99.995%), and He (99.999%) gas were obtained from Airgas, Inc. $^{13}CO_2$ gas (99%) was purchased from Cambridge Isotope Laboratories, Inc.

Quantitative ^{13}C-NMR (q-^{13}C-NMR) solvent was prepared as a 0.1 M solution of chromium acetylacetonate (obtained from Sigma-Aldrich) in DMSO-d6. NMR tubes (5 mm OD; 7″ L; wall thickness: 0.38 mm) with coded closed caps were purchased from Bruker. The water contents were measured by a Karl Fischer titrator (Metrohm Coulometric KF 889D) and were below 1000 ppm. Elemental analyses were performed at Atlantic Microlab.

Synthesis and Characterization of Reactive ILs. As reported previously for [EMIM][2-CNpyr],[32] ILs were synthesized in a two-step reaction starting from the halide version of the cation precursor salts, where the halide was converted into hydroxide by an anion exchange step and then reacted with anion precursors to get corresponding IL in the second step. Briefly, the chloride or the bromide versions of the cation salts were converted into the hydroxide form in methanol solution using the anion exchange resin. The anion exchange was carried out until no visual silver halide precipitation was observed by the silver nitrate test. The anion precursor was then added into the solution and stirred overnight at room temperature for the acid−base reaction to

https://doi.org/10.1021/acscatal.3c01538
ACS Catal. 2023, 13, 7812−7821

Table 1. Chemical Structures and Purities of ILs Studied[a]

ILs full name	abbreviation	structure	purity	supplier
1-Ethyl-3-methyl-imidazolium 2-cyanopyrrolide	[EMIM][2-CNpyr]	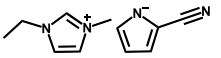	>98%	In-house synthesis
1-Ethyl-3-methyl-imidazolium chloride	[EMIM][Cl]	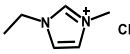	>98%	IoLiTec
1-Ethyl-3-methyl-imidazolium bis(trifluoromethyl-sulfonyl)imide	[EMIM][TFSI]	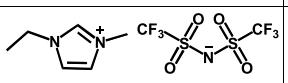	≥97%	IoLiTec
1-Ethyl- 2,3-dimethyl-imidazolium bis(trifluoromethyl-sulfonyl)imide	[EMMIM][2-CNpyr]	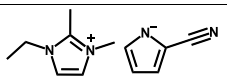	>98%	In-house synthesis
Choline 2-cyanopyrrolide	[Ch][2-CNpyr]	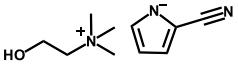	>98%	In-house synthesis

[a]Reported purities are determined by NMR for the synthesized samples and as provided by the supplier for commercial samples.

complete, thus forming the IL of interest (85 ± 5% yield) and the water by-product. The excess solvent and residual water were removed via rotary evaporation at 50 °C for an hour, and the sample was further dried under vacuum first for 1 day at room temperature and then 2 days at 50 °C.

For the synthesis of 1-ethyl-2,3-dimethyl imidazolium 2-cyanopyrrolide ([EMMIM][2-CNpyr]), the precursor [EMMIM][Br] was first synthesized via Menshutkin reaction. Briefly, 1,2-dimethylimidazole and 2-bromoethane in a 1:1.3 molar ratio were refluxed at 40 °C for 3 h under an inert atmosphere. The reaction mixture was cooled to room temperature, and the white crystals were immediately formed. The crystals were purified via first washing with ethyl acetate and then drying with diethyl ether to remove any unreacted reactants. The crystals were dried under vacuum at 60 °C for 3 days. Synthesized samples were confirmed by ^{1}H- and ^{13}C-nuclear magnetic resonance (NMR) spectroscopy (Bruker Ascend 500 MHz) in DMSO-d6 (Figures S1−S4). All NMR spectroscopy results were performed using the same instrument and solvent unless noted otherwise. The chemical structures and purities of the ILs are shown in Table 1. The halide content of the synthesized samples was determined by elemental analysis and reported to be less than the detection limit of the combustion ion chromatography (0.25%).

Electrochemical Measurements and Product Analysis. *Electrochemical Methods.* The linear sweep voltammograms (LSVs) were recorded at a potential sweep rate of 10 mV/s at room temperature (22 °C) in both the N_2- and CO_2-saturated electrolytes. LSV was performed to determine the onset potential for CO_2RR. LSVs were performed in a single-compartment glass cell using a three-electrode assembly at the ambient conditions. All glassware parts were cleaned and dried overnight at 110 °C. For the working and counter electrodes, Ag foil (0.38 cm^2 area) and Pt mesh (2 × 2 cm) were used, respectively. The silver working electrode was prepared by mechanical polishing of Ag foil using a series of abrasive sheets (3000, 5000, and 8000 grit), followed by cleaning ultrasonically in ethanol and water. The reference electrode was a nonaqueous Ag/Ag$^+$ electrode (0.01 M $AgNO_3$ and 0.1 M TEAP in acetonitrile). The reported potentials are IR corrected (V-IR$_\Omega$) by compensating 80% of the measured resistance with reference to Ag/Ag$^+$. The electrochemical cell was filled with 5 mL of electrolyte solution and purged with dry N_2 gas for at least 30 min prior to the experiments to remove O_2 traces. The CO_2 and N_2 flow rates in the electrochemical cell were maintained with a mass flow controller (Brooks Mass Flow Controller, North Coast Metrology, USA). To prevent moisture accumulation in the electrolyte due to the gas flow from the tanks, moisture traps (VICI Metronics) were installed on N_2 and CO_2 gas lines, which ensured <1 ppb moisture in the feed to the electrochemical cell. A mixture of 0.1 M TEAP in acetonitrile was used as the supporting electrolyte. Acetonitrile was dried with activated molecular sieves prior to use. The water content of the prepared electrolytes was determined by the Karl−Fischer titration, and for all of the samples, the water content was below 500 ppm.

Product Analysis. To identify the reaction products, electrolysis experiments were carried out under continuous purging of CO_2 at a flow rate of 10 mL/min while sampling the headspace of the single-compartment electrochemical cell. The gas outlet of the electrochemical cell was directly connected to a gas chromatography (GC, GC-7890B, Agilent Technologies) sampling valve for online gas sampling. The GC was equipped with six different columns and three detectors for simultaneous separation of CO, CO_2, H_2, and hydrocarbons. A thermal conductivity detector (TCD) and a flame ionization detector (FID) were used to perform the quantitative analysis of the gas phase products. The GC apparatus was calibrated for quantitative analysis of the gaseous products (i.e., CO and H_2) using a calibration gas obtained from Airgas, Inc. (USA). The calibration gas contains 5 mol % each of CO and 0.2 mol % of H_2 balanced in CO_2. The known volume of standard samples was automatically injected to GC using He and N_2 as carrier gases for detecting CO and H_2, respectively. A clear CO peak appeared at 7.85 min on TCD2B while H_2 was detected at 1.15 min on the TCD2C detector. The calibration curves were obtained based on the peak surface area with respect to the number of moles of the injected gases (i.e., CO and H_2), as shown in Figure S5. Finally, the molar quantity of products was calculated during the reduction reaction by correlating the product peak area with the obtained calibration curves.

The time needed to reach the steady-state concentration was approximately 15 min, so samples from bulk electrolysis

https://doi.org/10.1021/acscatal.3c01538
ACS Catal. 2023, 13, 7812−7821

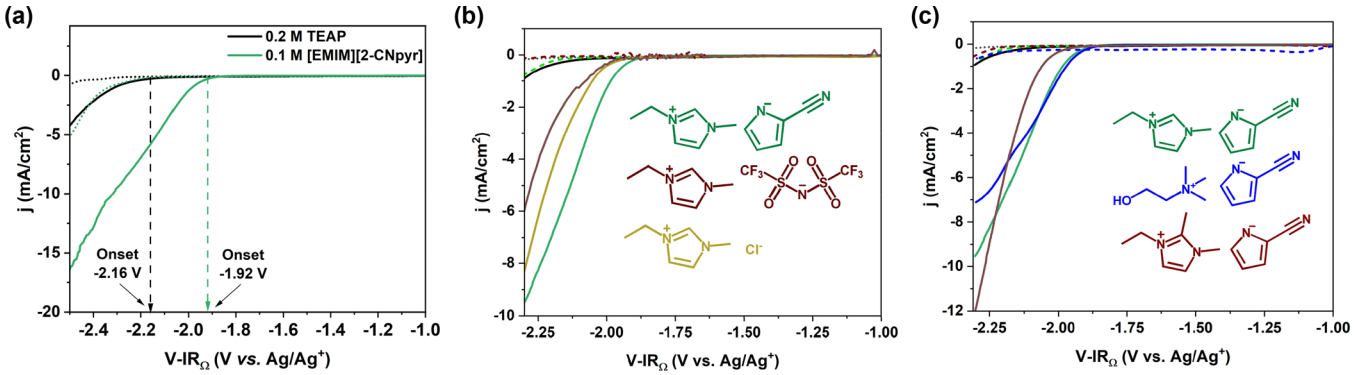

Figure 1. LSVs of electrolytes examined under N_2 (dotted lines) and CO_2 (solid lines). (a) 0.2 M TEAP in acetonitrile. (b) 0.1 M [EMIM][2-CNpyr] added to the supporting electrolyte of 0.1 M TEAP in acetonitrile. (c) [EMIM][TFSI] and [EMIM][Cl] and (d) [Ch][2-CNpyr] and [EMMIM][2-CNpyr], in comparison to [EMIM][2-CNpyr]; each are 0.1 M in concentration.

experiments were injected at every 20 min with an online gas sampling valve. The liquid products formed during the electrolysis were analyzed by NMR. The NMR samples were prepared by mixing 350 μL of DMSO-d6 solvent with 350 μL of electrolyte. The electrolyte obtained before and after CO_2RR was also characterized by ATR-FTIR using a Nicolet iS50 FTIR (Thermo Scientific) with 32 scans, at a resolution of 4 cm^{-1}, on a diamond crystal.

The Faradaic efficiency (FE) for CO_2RR gaseous products during the electrolysis experiments was calculated as follows:

$$\text{FE}\ (\%) = \frac{e_{\text{out}}}{e_{\text{in}}} \times 100 = \frac{yn}{Q/F} \times 100$$

where y is the measured amount of product in a 0.25 mL sample loop (based on calibration of the GC) with a standard gas (mol), n (=2) is the number of electrons required to form a molecule of CO or H_2, Q is the measured charge (C), and F is the Faraday constant (96,485 C/mol).

In Situ Raman Spectroscopy. In situ SERS measurements were performed with a homebuilt spectroscopic cell (Figure S6) and a Renishaw InVia spectrometer system with a 785 nm excitation laser source. The Ag foil, Pt coil, and Ag/Ag^+ were used as working, counter, and reference electrodes, respectively. To obtain SERS active Ag as the working electrode, the Ag foil was electrochemically roughened in 0.1 M KCl solution with a Pt mesh counter electrode and a Ag/AgCl reference electrode by applying three potential sweeps between 0.25 and −0.4 V (vs Ag/AgCl) to the working electrode with a 5 mV/s scan rate (Figure S7a).[33] The obtained Ag foil was then cleaned and dried to remove residual Cl and moisture from the surface. Scanning electron microscopy (SEM) and atomic force microscopy (AFM) were used to confirm the effectiveness of the roughening process. The SEM and AFM images of pristine Ag foil and electrochemically roughened Ag foil are shown in Figure S7b. The energy-dispersive X-ray (EDX) analysis (Figure S8) shows the absence of oxygen or any other compound, confirming that the roughened Ag surface is free from any impurities and oxides.

The Raman probe was focused on the electrode/electrolyte interface with a 20× microscope objective (LMPLFL Olympus, 20×, NA = 0.4,WD = 12 mm). Various combinations of acquisition times per spectrum (integration time) and laser power were evaluated. The high-quality potential-dependent spectral changes with minimum time duration were obtained using a 10 s laser exposer and 1 accumulation at 1% laser power. The resolution for the spectra collected between 300 and 3200 cm^{-1} is 0.5 cm^{-1}. The obtained SERS data was processed with Origin 2022 (version 9.9.0.225) software for background subtraction and peak normalization.

Electron Paramagnetic Resonance Spectroscopy. Electron paramagnetic resonance (EPR) spectroscopy was performed at the CalEPR center in the University of California, Davis. Samples were prepared following the procedure for constant potential electrolysis for the catalytic generation of CO from CO_2. After 30 min of electrolysis, 200 μL of electrolysis sample was removed from the cell with a syringe and injected into a N_2-filled EPR tube, which was then frozen in liquid nitrogen. X-band continuous-wave spectra were recorder on a Bruker BioSpin ELEXSYS E500 spectrometer equipped with a super high Q resonator (ER4122SHQE). Cryogenic temperatures were achieved by using an ESR900 liquid helium cryostat with a temperature controller (Oxford Instruments ITC503) and a gas flow controller. All CW-EPR spectra were recorded under slow-passage, non-saturating conditions. Spectrometer settings were as follows: conversion time = 60 ms, modulation frequency = 100 kHz, modulation amplitude = 0.2 mT, and other settings as given in the corresponding figure captions. The Q-Band Mims ENDOR spectrum was recorded on a Bruker BioSpin ELEXSYS-580 spectrometer with an R.A. Isaacson cylindrical TE011 resonator, a 10 W microwave amplifier, and a 1 kW LPI-10 RF amplifier. The pulse sequences employed were as follows: electron spin-echo detected field swept EPR (π/2-τ-π-τ-echo) and Mims ENDOR (π/2-τ-π/2-RF-π/2-τ-echo).

RESULTS AND DISCUSSION

The co-catalytic activity of [EMIM][2-CNpyr] is studied by LSV using the Ag working electrode (Figure 1). The onset potential for CO_2RR in the supporting electrolyte (0.1 M TEAP in acetonitrile) is observed at −2.16 V (vs Ag/Ag^+), as marked in Figure 1a. After addition of 0.1 M [EMIM][2-CNpyr] in this supporting electrolyte, the onset is shifted to −1.92 V (vs Ag/Ag^+). The 240 mV positive shift in onset potential suggests a reduction in the activation energy of CO_2. This can be explained by the reactivity of the IL with CO_2. It is reported previously that the CO_2 absorption by [EMIM][2-CNpyr] forms carbamate (−N−COO^-) and carboxylate (−C−COO^-) species through binding to the anion and cation (via carbene intermediate), respectively, under anhydrous conditions.[32] Similarly, in this study, the same products

https://doi.org/10.1021/acscatal.3c01538
ACS Catal. 2023, 13, 7812−7821

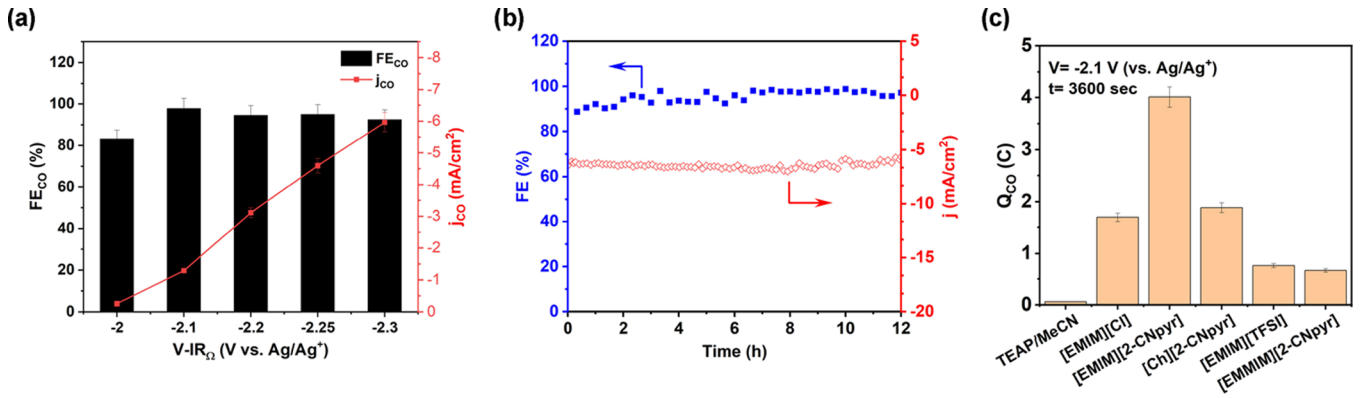

Figure 2. (a) Faradaic efficiency (FE_{CO}) and partial current density of CO (j_{CO}) at different potentials during CO_2RR over Ag with 0.1 M [EMIM][2-CNpyr] in the supporting electrolyte. (b) Faradaic efficiencies (filled blue squares) for CO production and total current density (red hollow diamonds) during 12 h of continuous CO_2RR with 0.1 M [EMIM][2-CNpyr] in the supporting electrolyte on the Ag electrode at −2.2 V vs Ag/Ag^+. (c) Comparison of the charge consumed for CO generation (Q_{CO}) measured upon electrolysis at −2.1 V vs Ag/Ag^+ for 1 h among the ILs studied. TEAP/MeCN is 0.2 M TEAP in acetonitrile. ILs were introduced to the supporting electrolyte of 0.1 M TEAP in acetonitrile at 0.1 M concentration.

are confirmed by ^1H and ^{13}C NMR for [EMIM][2-CNpyr] in acetonitrile (Figures S9 and S10). When the concentration of [EMIM][2-CNpyr] is increased, the CO_2RR onset potential stays about the same, as seen in Figure S11. However, the current increases as the IL concentration increases from 0.1 to 1 M and then decreases as it reaches to 1.5 and 2 M. At higher concentrations, viscosities substantially increase (Figure S12), thus presenting mass transfer limitations. This dependence on IL concentration could also be related to the changes in the double-layer structure where surface coverage by $[EMIM]^+$ is more pronounced at higher concentrations, as previously discussed by Liu et al. for $[EMIM][BF_4]$ in acetonitrile.[34]

Due to the availability of multiple CO_2 binding sites, it is difficult to comment on the most active species responsible for the observed co-catalytic activity for CO_2RR. Therefore, we further performed LSV measurements by changing the anion and cation structures in a systematic way to probe the role of these CO_2 complexes. In the first set of experiments, we studied the effect of the anion on onset potential by examining the imidazolium ILs with $[Cl]^-$ and $[TFSI]^-$ in comparison to $[2\text{-CNpyr}]^-$. The lowest CO_2RR onset potential was with [EMIM][2-CNpyr], as seen in Figure 1b. In the second set of experiments, the impact of the cation was investigated by comparing [EMIM][2-CNpyr] to [Ch][2-CNpyr] and [EMMIM][2-CNpyr]. This experiment revealed identical catalytic onset potentials for $[EMIM]^+$ and $[Ch]^+$ and similar current densities for both ILs in acetonitrile, as shown in Figure 1c. In addition, we found that when the carbene route for CO_2 binding is eliminated by blocking it with a methyl group on the imidazolium C2 carbon ($[EMMIM]^+$), the onset potential is slightly more negative compared to [EMIM][2-CNpyr] for CO_2RR but still more positive compared to the supporting electrolyte itself. These results confirm that $[2\text{-CNpyr}]^-$ also plays a significant role in the observed catalytic enhancement in addition to $[EMIM]^+$.

To investigate the product identity from CO_2RR in the presence of the synthesized ILs in acetonitrile (0.1 M IL with 0.1 M TEAP-supporting salt), bulk electrolysis experiments were performed on the Ag electrode (0.38 cm^2) in a single compartment cell. Online gas sampling during the bulk electrolysis experiment showed CO as the only gaseous product in all of the systems studied. Figure 2a shows the obtained FE for CO at different applied potentials for 1 h with [EMIM][2-CNpyr]. A maximum selectivity of 94% for CO was achieved at −2.1 V (vs Ag/Ag^+). A very stable current response was obtained at the applied potentials between −2.0 and −2.3 V (vs Ag/Ag^+), as seen in Figure S13. More importantly, high-resolution ^1H NMR spectroscopic analysis of the electrolyte post electrolysis showed no evidence of the degradation of [EMIM][2-CNpyr] after 1−3 h (Figure S9) of continuous CO_2RR.

The long-term stability of the [EMIM][2-CNpyr] containing electrolyte was further evaluated by running the CO_2 reduction experiment continuously for 12 h at −2.2 V. As shown in Figure 2b, the Faradaic efficiency for CO stays around >94% during the course of CO_2RR. The electrolyte after 12 h of CO_2RR was analyzed by NMR (^{13}C NMR in Figure S14) and ATR-FTIR (Figure S15) where spectral changes are clearly seen, compared to 1−3 h of CO_2RR. While the exact mechanism by which degradation occurs is unknown, ^1H NMR analysis, summarized in Table S1, indicates decreased anion peak intensities possibly due to degradation or volatilization of the protonated anion (2-CNpyrH). This specie, which was formed during CO_2 absorption, can interact with either the carboxylate or the carbamate adducts. In the case of the neat IL, these close interactions prevent the escape of 2-CNpyrH from the liquid phase. However, during CO_2RR in acetonitrile, evaporative escape of 2-CNpyrH is possible.

The CO_2RR performance in the presence of other ILs are presented in Figure 2c in terms of the charge utilized for CO production during the electrolysis at −2.1 V (vs Ag/Ag^+) for 1 h. The charge utilization for CO production by the electrolyte containing [EMIM][2-CNpyr] is the highest among the studied ILs. Even when compared to [Ch][2-CNpyr], which has a similar onset potential (Figure 1c), the total charge utilized for CO production with [EMIM][2-CNpyr] is dramatically higher at −2.1 V (vs Ag/Ag^+) in 1 h. We attribute this enhancement by [EMIM][2-CNpyr] for CO_2RR due to its superior CO_2 sorption[32] and multiple proton sources to facilitate CO_2RR[35−37] in comparison to other ILs studied.[38,39] The CO selectivity with [EMIM][2-CNpyr] over the Ag surface is comparable with the other [EMIM]-based ILs reported recently (Table S2); however, the proton source and the mechanism are different here where a robust

https://doi.org/10.1021/acscatal.3c01538
ACS Catal. 2023, 13, 7812−7821

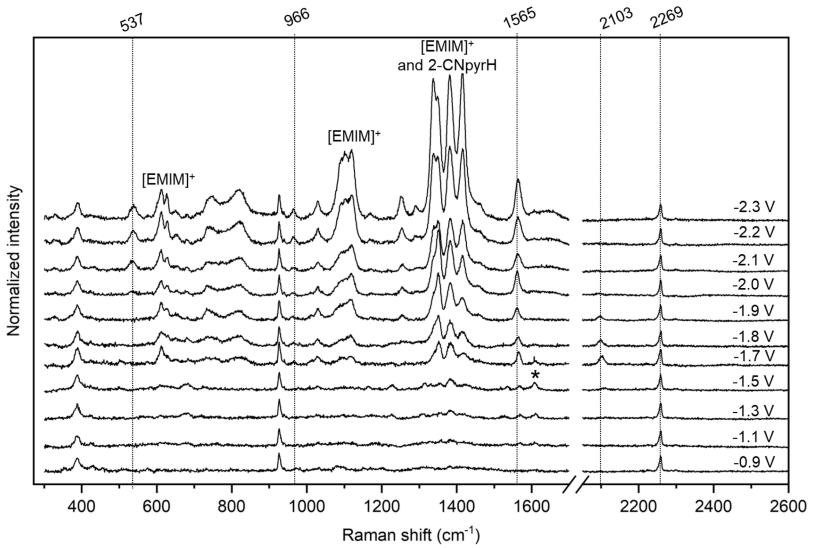

Figure 3. Potential-dependent SERS on an electrochemically roughened Ag electrode with the CO_2-saturated electrolyte: 0.1 M [EMIM][2-CNpyr] and 0.1 M TEAP in acetonitrile. Potentials are with respect to Ag/Ag^+.

electrolysis can be achieved due to the stability of the intermediates at the electrode surface, as explained by SERS analysis.

Literature suggests that the co-catalytic activity of [EMIM]-based ILs in CO_2RR primarily originates from the complexation of the imidazolium cation and CO_2. The [EMIM]−CO_2 complex was suggested to lower the energy barrier for the formation of the $CO_2^{\bullet-}$ radical anion and to suppress the competing reaction of H_2 production by forming a monolayer on the cathode. However, in the presence of the basic [2-CNpyr]$^-$, CO_2 chemically binds to the anion. Furthermore, some of the [2-CNpyr]$^-$ get protonated by the hydrogen on the C2 carbon of the imidazolium, thus forming a carbene that also binds with CO_2 prior to reduction of CO_2 to $CO_2^{\bullet-}$. Since CO_2 is transformed from a linear form to a bent geometry by binding to [EMIM][2-CNpyr], the chemical reaction complexes are believed to serve as the co-catalysts, thus lowering the onset potential. In order to identify the electrode surface species during CO_2RR and capture the role of the ions, SERS measurements were performed, as seen in Figure 3. The peak at 2269 cm^{-1} is the CN stretching of acetonitrile, and this was used as an internal reference and spectral normalization. At open circuit potential (OCP), −0.9 V, as molecules are randomly arranged on the electrode surface, there are not many distinct features besides the acetonitrile peaks. With increased negative polarization, significant spectral changes are visible with the most significant ones due to the enrichment of the electrode surface with [EMIM]$^+$ (1336, 1348, 1380, 1415 cm^{-1}).[40,41] This observation is consistent with the earlier reports where surface adsorption of [EMIM]$^+$ on Ag nanoparticles was observed (with counter ions of $[BF_4]^-$[34] and $[Cl]^-$[41]). This shows that the imidazolium cation starts breaking the solvation barrier at about −1.5 V (vs Ag/Ag^+) and start to adsorb on the Ag surface. It should be noted that [EMIM]$^+$ enrichment is only seen with a SERS active Ag surface; Figure S16 shows no spectral changes with a smooth Ag surface due to bulk interference and lack of spectral enhancement. Furthermore, [EMIM]$^+$ migration to the surface is seen even in the absence of CO_2 on SERS surface upon negative polarization as seen in Figure S17, with slight differences in the spectral shapes under N_2. Additionally, it is possible that some features related to the anion or 2-CNpyrH (e.g., CNC in-phase stretch, C═C stretch, and out-of-phase C═C stretch) can overlap with the [EMIM]$^+$ features in the region of 1380−1460 cm^{-1}.[42] Because the concentration of the anionic specie is low at the negatively polarized surface, it is difficult to observe it by SERS. However, stretching of C≡N (υ(CN)) of [2-CNpyr]$^-$ under N_2 is observed at 2190 cm^{-1} when the IL concentration is increased to 0.5 M in the supporting electrolyte. This vibration shows a blue shift by 33 cm^{-1} after CO_2 saturation, as seen in Figure S18, which is interpreted to be due to the [2-CNpyr]-CO_2 complex (carbamate).

Another important feature seen in Figure 3 is the C≡O stretching mode of CO_{ad} at 2103 cm^{-1}. This new peak emerges at a potential of −1.7 vs Ag/Ag^+, consistent with previous literature where CO surface adsorption is reported.[43−45] This peak is absent under N_2, as shown in Figure S19. The 2103 cm^{-1} peak shifts to lower wavenumbers and decreases in intensity as the potential is swept more negative, demonstrating a Stark shift of 26 cm^{-1} V^{-1} (Figure S20), which is consistent with ca. 21 cm^{-1} V^{-1} in literature.[46] Both the reduction in intensity and the redshift in SERS can be explained in terms of surface coverage reduction of CO_{ad} and the desorption of CO from the surface with increased polarization as identified by GC analysis upon electrolysis.

There are other emerging vibrations under CO_2, as indicated along the dotted lines in Figure 3. As the electrode is negatively polarized to −1.1 V, a new peak at 1612 cm^{-1} appears (marked with * in Figure 3 where its intensity is highest) and can be assigned to $\upsilon_{as}(CO_2^-)$, likely of the carboxylate via the carbene intermediate.[42,44] This feature is visible up to −1.7 V and then diminishes as the peak at 1565 cm^{-1} intensifies. Although the 1565 cm^{-1} peak is also seen in SERS under N_2 at −1.8 V (Figure S17b), its appearance is more prominent under CO_2 saturation and at an earlier potential at −1.1 V. Therefore, there could be two explanations: one where the IL ions are reorienting or breaking solvation and another where [EMIM]$^+$-COOH forms.[43,47] Other features related to −COOH at 966 cm^{-1} (out-of-plane bending of OH of COOH) and 537 cm^{-1} (CO of COOH out-of-plane deformation) are previously reported at CO_2RR potentials.[42] As illustrated in Figure 4,

https://doi.org/10.1021/acscatal.3c01538
ACS Catal. 2023, 13, 7812−7821

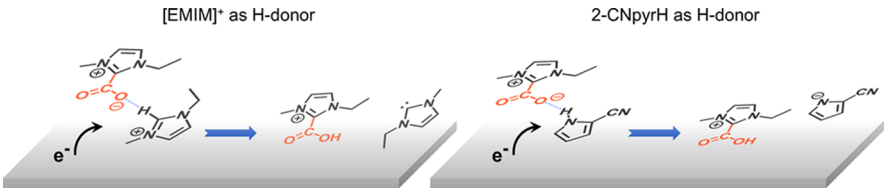

Figure 4. Illustration of the possible interactions on the electrode surface. Left: Electron injection to the $[EMIM]^+$ on the surface coupled with a proton transfer from $[EMIM]^+$ to $[EMIM]^+$-CO_2^- generates carbene and $[EMIM]^+$-COOH. Right: Electron injection to the 2-CNpyrH (protonated anion from CO_2 absorption reaction) on the surface coupled with a proton transfer to $[EMIM]^+$-CO_2^- generates $[2\text{-CNpyr}]^-$ and $[EMIM]^+$-COOH.

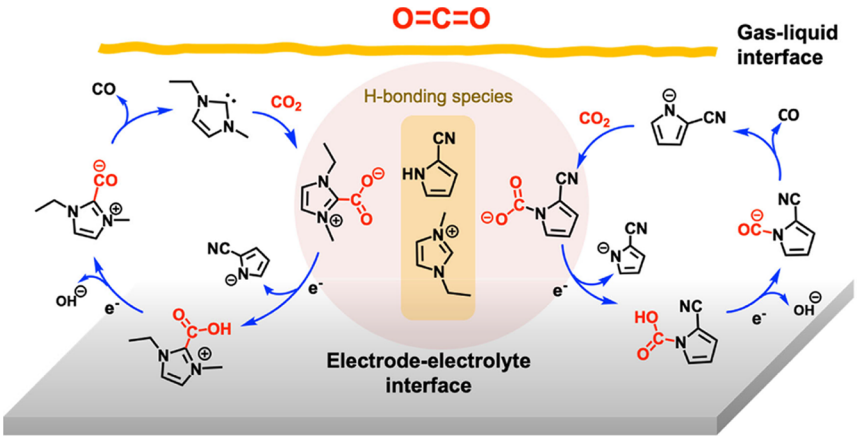

Figure 5. Illustration of CO_2 absorption by the [EMIM][2-CNpyr] based non-aqueous electrolyte and the proposed reaction schemes for CO_2RR at the electrode−electrolyte interface. The structures highlighted in the middle by the colored circle correspond to the post CO_2 capture species (carboxylate, carbamate, $[EMIM]^+$, and the protonated anion, 2-CNpyrH). The two possible reaction routes demonstrate the role of the CO_2-reactive ions in co-catalyzing CO generation as understood from the combined electrochemistry and spectroscopy analysis. $[EMIM]^+$ and 2-CNpyrH have protons that can transfer to the carboxylate or the carbamate to carboxylic acid species. However, it is more likely that 2-CNpyrH is the proton source in this case; therefore, $[2\text{-CNpyr}]^-$ release from the surface by the first electron transfer is illustrated.

there are multiple possible proton sources for this complex to form: C2 proton of $[EMIM]^+$ ($pK_{a(H2O)} \sim 23$)[48] and −NH proton of 2-CNpyrH ($pKa_{(H2O)} \sim 15$).[49] The lower pK_a of 2-CNpyrH makes it more likely being a proton donor. Upon electron injection, both the hydrogen on the C2 carbon of $[EMIM]^+$ on the surface and 2-CNpyrH close to the surface may transfer proton to the $[EMIM]^+$-CO_2^- adduct on the surface, thus releasing carbene and $[2\text{-CNpyr}]^-$ while forming $[EMIM]^+$-COOH. It is possible that there are additional steps to the mechanism where hydrogen is first adsorbed on the surface upon reduction of $[EMIM]^+$ or 2-CNpyrH and then combining with $[EMIM]^+$-CO_2^-.

To better understand the role of 2-CNpyrH, LSV and SERS experiments were performed by intentionally adding the neutral 2-CNpyrH (0.5 M) to the supporting electrolyte (Figure S21). Current density increased at −1.45 V (vs Ag/Ag^+), which is ascribed to the reduction of 2-CNpyrH forming the anion $[2\text{-CNpyr}]^-$ and H^+. In SERS, it is seen that the intensity of the 2230 cm^{-1} peak (CN stretch) increased with polarization up to −2.2 V (vs Ag/Ag^+), thus confirming the increased surface concentration of the pyrrole, which can act as the proton source in CO_2RR. However, the in situ SERS setup is not time-resolved to capture the short-lived intermediates to identify the exact mechanism. On the other hand, the FTIR analysis post CO_2RR confirms the existence of carboxylic acid that was not in the solution prior to electrolysis as seen in Figure S15. The surface-adsorbed carboxylic acid complex ($[EMIM]^+$-COOH) can further undergo electro-reduction to form surface-absorbed CO and OH^-. Wang et al. reported the favorable CO_2RR pathways with $[EMIM][BF_4]$ IL and the possibility of $[EMIM]^+$-CO^- as an intermediate following $[EMIM]^+$-COOH formation, similar to this study.[36] Therefore, we hypothesize the overall CO_2RR reaction to be as shown in Figure 5.

An effective probe for detecting organic radical reaction intermediates generated in a solution is EPR spectroscopy. We therefore undertook a series of experiments to collect samples from electrolysis experiments performed under 1 atm N_2, CO_2, and $^{13}CO_2$. Aliquots of the electrolysis solution were removed from the sealed electrolysis cell after 30 min of electrolysis at −2.1 V vs Ag/Ag^+ using a gas-tight syringe and transferred to an N_2-filled EPR tube, which was then immediately frozen in liquid N_2. The sample collected from electrolysis under N_2 showed a very weak isotropic signal at g = 2.003, which indicated a small amount of a radical organic species in solution when probed at 45 K (Figure 6). The sample collected from electrolysis under CO_2 or $^{13}CO_2$ showed an isotropic signal with the same g value, but the signal was much higher in intensity. No discernable difference was found in CW EPR on the solutions collected under CO_2 vs $^{13}CO_2$. We did not detect N hyperfine coupling in any of the samples, which suggests that the radical is localized at a C-atom, in alignment with the proposed mechanism in Figure 5 where the radical is the imidazolium carbene. The higher intensity of the EPR signal observed under CO_2 may be correlated with the current density, which was roughly six times higher under CO_2 as compared with electrolysis run under 1 atm N_2, and that higher current density likely arises from faster generation of organic

https://doi.org/10.1021/acscatal.3c01538
ACS Catal. 2023, 13, 7812−7821

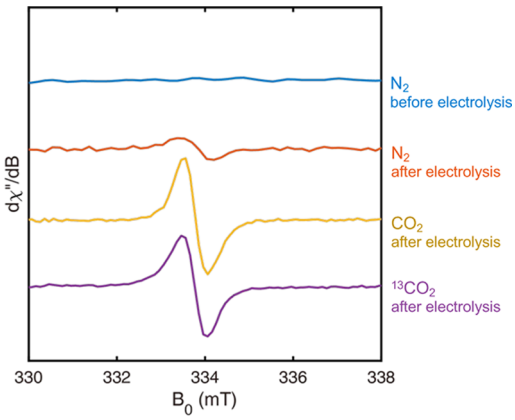

Figure 6. X-band continuous-wave EPR spectrum of 0.1 M [EMIM][2-CNpyr] in the supporting electrolyte, before electrolysis under N_2 and after electrolysis at −2.1 V vs Ag/Ag^+ under N_2, CO_2, and $^{13}CO_2$ environment. The CO_2-saturated electrolyte before electrolysis is not shown as it is the same as the top curve under N_2. There were no observable differences between the samples made from CO_2 and $^{13}CO_2$. EPR conditions: temperature = 45 K; microwave power = 0.02 mW; modulation amplitude = 0.2 mT.

radicals due to the follow-up reactions with CO_2 to liberate CO. We further analyzed the solutions obtained from electrolysis under $^{13}CO_2$ using electron nuclear double resonance spectroscopy (ENDOR). We did not observe ^{13}C hyperfine coupling in the Q-band (34 GHz) Mims ENDOR spectrum, and this suggested that there is no radical character associated with CO_2 or with CO_2 bound to the organic radical.

Finally, the impact of water on CO_2RR was studied by varying the water content of the electrolyte. It is well-known that most of ILs are hygroscopic and may contain some residual water despite rigorous drying procedures. The presence of water (a proton source) in the IL can potentially lead to enhanced reaction rates via proton-coupled electron-transfer pathways. Our results show that the effect of adding water up to 1 vol % does not change the CO_2RR onset potential or the current as seen in Figure 7a. Further increase of water content to 8 vol % causes a positive shift in onset potentials, which could be due to the competing HER. Bulk electrolysis experiments with water containing electrolytes show an increase in current with increased water content at −2.2. V vs Ag/Ag^+, as in Figure 7b. This is accompanied by increased selectivity (FE) for CO from 94 to 98% when water content increased from less than 0.1 to 1 vol %, as shown in Figure 7c. Further increase of water content to 8 vol % results in the reduction of CO selectivity to 84% as a result of parallel H_2 evolution reaction. Our previous work reports on the bicarbonate formation upon CO_2 absorption by [EMIM][2-CNpyr] in the presence of water.[32] Bicarbonate acts as a proton donor for CO_2RR and HER, thus resulting in CO and H_2, respectively, on Ag.[50] These results imply that even in the presence of water up to 1 vol %, the electrode surface is covered with IL ions, thus suppressing HER.

CONCLUSIONS

The CO_2-reactive IL, [EMIM][2-CNpyr], was demonstrated as a catalytic electrolyte component for the electro-reduction of CO_2 to CO on the Ag surface. A high selectivity (>94%) and a stable current density for at least 12 h were achieved. These enhancements over a conventional acetonitrile-based electrolyte reveal the role of the carbamate and carboxylate species that form by the binding of CO_2 to $[2\text{-CNpyr}]^-$ and $[EMIM]^+$, respectively. The spectro-electrochemical studies further revealed the role of these species on CO_2RR at the electrode surface. In particular, the enrichment of surface species of $[EMIM]^+$, 2-CNpyrH, and $[EMIM]^+$-CO_2^-, as captured by SERS between the applied potentials of −1.6 to −2.3 V vs Ag/Ag^+, suggests the stabilization of the reaction intermediates and support the proposed reaction mechanism involving a radical formation as detected by EPR. The generation of CO on Ag was observed in SERS and CO was detected by the in-line gas chromatography during electrolysis. This study also demonstrated that the heterocyclic anion contributes to lowering of the CO_2RR onset potential. These findings serve as a basis for improved mechanistic understanding of CO_2RR in the presence of reactive ILs involving a basic anion.

ASSOCIATED CONTENT

Supporting Information

The Supporting Information is available free of charge at https://pubs.acs.org/doi/10.1021/acscatal.3c01538.

^1H and ^{13}C NMR spectra for all compounds; characterization of the SERS electrode by SEM and EDX; FTIR and NMR analyses of liquidous products of CO_2RR; GC calibration curve used for gaseous product analysis; SERS analysis of the control experiments; a comparison table of the examined electrolyte with literature for CO_2RR (PDF)

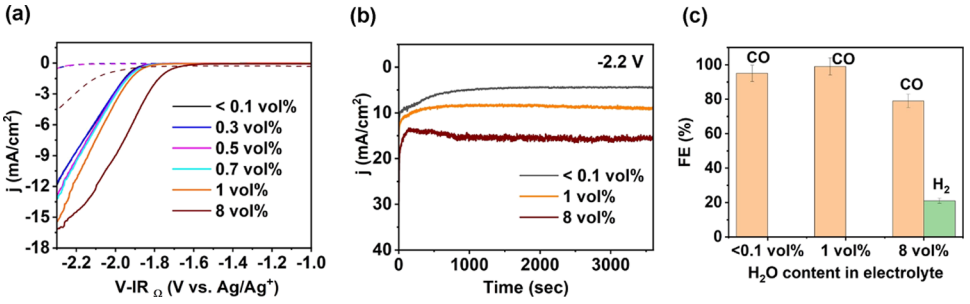

Figure 7. LSV of 0.1 M [EMIM][2-CNpyr] in supporting electrolyte showing the effect of water content on the onset potential (a); chronoamperometry at −2.2 V vs Ag/Ag^+ with samples containing 0.1, 1, and 8 vol % water (b); Faradaic efficiencies measured from chronoamperometry shown in b (c). Gaseous product composition was determined by GC (orange bars are for CO and green bar is for H_2).

https://doi.org/10.1021/acscatal.3c01538
ACS Catal. 2023, 13, 7812−7821

AUTHOR INFORMATION

Corresponding Author

Burcu Gurkan − *Chemical and Biomolecular Engineering, Case Western Reserve University, Cleveland, Ohio 44106, United States;* orcid.org/0000-0003-4886-3350; Email: beg23@case.edu

Authors

Saudagar Dongare − *Chemical and Biomolecular Engineering, Case Western Reserve University, Cleveland, Ohio 44106, United States;* orcid.org/0000-0001-6782-0028

Oguz Kagan Coskun − *Chemical and Biomolecular Engineering, Case Western Reserve University, Cleveland, Ohio 44106, United States;* orcid.org/0000-0002-8452-8552

Eda Cagli − *Chemical and Biomolecular Engineering, Case Western Reserve University, Cleveland, Ohio 44106, United States*

Kevin Y. C. Lee − *Department of Chemistry, University of California, Davis, Davis, California 95616, United States*

Guodong Rao − *Department of Chemistry, University of California, Davis, Davis, California 95616, United States*

R. David Britt − *Department of Chemistry, University of California, Davis, Davis, California 95616, United States;* orcid.org/0000-0003-0889-8436

Louise A. Berben − *Department of Chemistry, University of California, Davis, Davis, California 95616, United States;* orcid.org/0000-0001-6461-1829

Complete contact information is available at: https://pubs.acs.org/10.1021/acscatal.3c01538

Author Contributions

S.D. performed electrochemical measurements and analysis. O.K.C. built the SERS cell to perform the spectro-electrochemical measurements. E.C. synthesized the precursors and ionic liquids and caried out the NMR and ATR-FTIR analyses. K.Y.C.L. conducted the EPR experiments on in situ generated reaction intermediates from electrolysis experiments, and G.R. assisted with collection of EPR data. L.A.B. conceptualized the EPR characterization of samples, and R.D.B. provided expertise in interpretation of EPR data. B.G. conceptualized the study, contributed to the discussions of the results, and oversaw the project. All authors contributed to the writing of the manuscript.

Notes

The authors declare no competing financial interest.

ACKNOWLEDGMENTS

This study was funded by an NSF CAREER award (no. 2045111) from the Division of Chemical, Bioengineering, Environmental and Transport Systems (CBET), Interfacial Engineering and Electrochemical Systems. The authors acknowledge the donors of the American Chemical Society Petroleum Research Fund (Grant No. PRF 59520-DNI4) for partial support of S.D. to perform electrolysis experiments and U.S. Department of Energy, Basic Energy Sciences (award no. DE-SC0022214) for support for E.C. to perform synthesis and NMR analysis. L.A.B. thanks the DOE EFRC-funded Center for Closing the Carbon Cycle for support of work with award DE-SC0023427; this supported EPR studies of electrolysis experiments. The authors would like to thank the NMR Instrumentation Facility at the Department of Chemistry at Case Western Reserve University. The use of EPR instrumentation was funded by the National Institutes of Health Grant R35GM126961 to R.D.B.

REFERENCES

(1) Skrable, K.; Chabot, G.; French, C. World atmospheric CO_2, its 14C specific activity, non-fossil component, anthropogenic fossil component, and emissions (1750−2018). *Health Phys.* **2022**, *122*, 291−305.

(2) Tans, P. *Trends in Atmospheric Carbon Dioxide, Mauna Loa Observatory, Hawaii*. www.esrl.noaa.gov/gmd/ccgg/trends/, 2022.

(3) Roy, S.; Cherevotan, A.; Peter, S. C. Thermochemical CO_2 Hydrogenation to Single Carbon Products: Scientific and Technological Challenges. *ACS Energy Lett.* **2018**, *3*, 1938−1966.

(4) Zhang, Q.; Bown, M.; Pastor-Pérez, L.; Duyar, M. S.; Reina, T. R. CO_2 Conversion via Reverse Water Gas Shift Reaction Using Fully Selective Mo−P Multicomponent Catalysts. *Ind. Eng. Chem. Res.* **2022**, *61*, 12857−12865.

(5) Appel, A. M.; Bercaw, J. E.; Bocarsly, A. B.; Dobbek, H.; DuBois, D. L.; Dupuis, M.; Ferry, J. G.; Fujita, E.; Hille, R.; Kenis, P.; Kerfeld, C. A.; Morris, R. H.; Peden, C. H. F.; Portis, A. R.; Ragsdale, S. W.; Rauchfuss, T. B.; Reek, J. N. H.; Seefeldt, L. C.; Thauer, R. K.; Waldrop, G. L. Frontiers, opportunities, and challenges in biochemical and chemical catalysis of CO_2 fixation. *Chem. Rev.* **2013**, *113*, 6621−6658.

(6) Fujita, E.; Grills, D. C.; Manbeck, G. F.; Polyansky, D. E. Understanding the Role of Inter- and Intramolecular Promoters in Electro- and Photochemical CO_2 Reduction Using Mn, Re, and Ru Catalysts. *Acc. Chem. Res.* **2022**, *55*, 616−628.

(7) Del Vecchio, A.; Caillé, F.; Chevalier, A.; Loreau, O.; Horkka, K.; Halldin, C.; Schou, M.; Camus, N.; Kessler, P.; Kuhnast, B.; Taran, F.; Audisio, D. Late-Stage Isotopic Carbon Labeling of Pharmaceutically Relevant Cyclic Ureas Directly from CO_2. *Am. Ethnol.* **2018**, *130*, 9892−9896.

(8) Sullivan, I.; Goryachev, A.; Digdaya, I. A.; Li, X.; Atwater, H. A.; Vermaas, D. A.; Xiang, C. Coupling electrochemical CO_2 conversion with CO_2 capture. *Nat. Catal.* **2021**, *4*, 952−958.

(9) Nielsen, D. U.; Hu, X.-M.; Daasbjerg, K.; Skrydstrup, T. Chemically and electrochemically catalysed conversion of CO_2 to CO with follow-up utilization to value-added chemicals. *Nat. Catal.* **2018**, *1*, 244−254.

(10) Kuhl, K. P.; Hatsukade, T.; Cave, E. R.; Abram, D. N.; Kibsgaard, J.; Jaramillo, T. F. Electrocatalytic Conversion of Carbon Dioxide to Methane and Methanol on Transition Metal Surfaces. *J. Am. Chem. Soc.* **2014**, *136*, 14107−14113.

(11) Tang, S.; Zhou, X.; Zhang, S.; Li, X.; Yang, T.; Hu, W.; Jiang, J.; Luo, Y. Metal-Free Boron Nitride Nanoribbon Catalysts for Electrochemical CO_2 Reduction: Combining High Activity and Selectivity. *ACS Appl. Mater. Interfaces* **2019**, *11*, 906−915.

(12) Li, J.; Zitolo, A.; Garcés-Pineda, F. A.; Asset, T.; Kodali, M.; Tang, P.; Arbiol, J.; Galán-Mascarós, J. R.; Atanassov, P.; Zenyuk, I. V.; Sougrati, M. T.; Jaouen, F. Metal Oxide Clusters on Nitrogen-Doped Carbon are Highly Selective for CO_2 Electroreduction to CO. *ACS Catal.* **2021**, *11*, 10028−10042.

(13) Fan, L.; Xia, C.; Yang, F.; Wang, J.; Wang, H.; Lu, Y. Strategies in catalysts and electrolyzer design for electrochemical CO_2 reduction toward C_{2+} products. *Science* **2020**, *6*, No. eaay3111.

(14) Zhang, S.; Fan, Q.; Xia, R.; Meyer, T. J. CO_2 Reduction: From Homogeneous to Heterogeneous Electrocatalysis. *Acc. Chem. Res.* **2020**, *53*, 255−264.

(15) Hanc-Scherer, F. A.; Montiel, M. A.; Montiel, V.; Herrero, E.; Sánchez-Sánchez, C. M. Surface structured platinum electrodes for the electrochemical reduction of carbon dioxide in imidazolium based ionic liquids. *Phys. Chem. Chem. Phys.* **2015**, *17*, 23909−23916.

(16) Matsubara, Y.; Grills, D. C.; Kuwahara, Y. Thermodynamic aspects of electrocatalytic CO_2 reduction in acetonitrile and with an ionic liquid as solvent or electrolyte. *ACS Catal.* **2015**, *5*, 6440−6452.

(17) Tan, X.; Sun, X.; Han, B. Ionic Liquid-Based electrolytes for CO_2 electroreduction and CO_2 electroorganic transformation. *Natl. Sci. Rev.* **2022**, *9*, No. nwab022.
(18) Welch, L. M.; Vijayaraghavan, M.; Greenwell, F.; Satherley, J.; Cowan, A. J. Electrochemical carbon dioxide reduction in ionic liquids at high pressure. *Faraday Discuss.* **2021**, *230*, 331−343.
(19) Rosen, B. A.; Salehi-Khojin, A.; Thorson, M. R.; Zhu, W.; Whipple, D. T.; Kenis, P. J.; Masel, R. I. Ionic liquid−mediated selective conversion of CO_2 to CO at low overpotentials. *Science* **2011**, *334*, 643−644.
(20) Rosen, B. A.; Haan, J. L.; Mukherjee, P.; Braunschweig, B.; Zhu, W.; Salehi-Khojin, A.; Dlott, D. D.; Masel, R. I. In situ spectroscopic examination of a low overpotential pathway for carbon dioxide conversion to carbon monoxide. *J. Phys. Chem. C* **2012**, *116*, 15307−15312.
(21) Ratschmeier, B.; Kemna, A.; Braunschweig, B. Role of H_2O for CO_2 Reduction Reactions at Platinum/Electrolyte Interfaces in Imidazolium Room-Temperature Ionic Liquids. *ChemElectroChem* **2020**, *7*, 1765−1774.
(22) Ratschmeier, B. r.; Braunschweig, B. r. Cations of Ionic Liquid Electrolytes Can Act as a Promoter for CO_2 Electrocatalysis through Reactive Intermediates and Electrostatic Stabilization. *J. Phys. Chem. C* **2021**, *125*, 16498−16507.
(23) Ratschmeier, B.; Braunschweig, B. Role of imidazolium cations on the interfacial structure of room-temperature ionic liquids in contact with Pt (111) electrodes. *Electrochem. Sci. Adv.* **2022**, No. e2100173.
(24) Zhao, Y.; Liu, X.; Lei, D. Y.; Chai, Y. Effects of surface roughness of Ag thin films on surface-enhanced Raman spectroscopy of graphene: spatial nonlocality and physisorption strain. *Nanoscale* **2014**, *6*, 1311−1317.
(25) Golru, S. S.; Biddinger, E. J. Effect of anion in diluted imidazolium-based ionic liquid/buffer electrolytes for CO_2 electroreduction on copper. *Electrochim. Acta* **2020**, *361*, No. 136787.
(26) Kang, X.; Zhu, Q.; Sun, X.; Hu, J.; Zhang, J.; Liu, Z.; Han, B. Highly efficient electrochemical reduction of CO_2 to CH_4 in an ionic liquid using a metal−organic framework cathode. *Chem. Sci.* **2016**, *7*, 266−273.
(27) Rosen, B. A.; Zhu, W.; Kaul, G.; Salehi-Khojin, A.; Masel, R. I. Water Enhancement of CO_2 Conversion on Silver in 1-Ethyl-3-Methylimidazolium Tetrafluoroborate. *J. Electrochem. Soc.* **2013**, *160*, H138−H141.
(28) Chen, L.; Guo, S.-X.; Li, F.; Bentley, C.; Horne, M.; Bond, A. M.; Zhang, J. Electrochemical Reduction of CO_2 at Metal Electrodes in a Distillable Ionic Liquid. *ChemSusChem* **2016**, *9*, 1271−1278.
(29) Hollingsworth, N.; Taylor, S. R.; Galante, M. T.; Jacquemin, J.; Longo, C.; Holt, K. B.; De Leeuw, N. H.; Hardacre, C. Reduction of carbon dioxide to formate at low overpotential using a superbase ionic liquid. *Angew. Chem., Int. Ed.* **2015**, *54*, 14164−14168.
(30) Sun, L.; Ramesha, G. K.; Kamat, P. V.; Brennecke, J. F. Switching the Reaction Course of Electrochemical CO_2 Reduction with Ionic Liquids. *Langmuir* **2014**, *30*, 6302−6308.
(31) Tanner, E. E. L.; Batchelor-McAuley, C.; Compton, R. G. Carbon Dioxide Reduction in Room-Temperature Ionic Liquids: The Effect of the Choice of Electrode Material, Cation, and Anion. *J. Phys. Chem. C* **2016**, *120*, 26442−26447.
(32) Lee, Y.-Y.; Edgehouse, K.; Klemm, A.; Mao, H.; Pentzer, E.; Gurkan, B. Capsules of reactive ionic liquids for selective capture of carbon dioxide at low concentrations. *ACS Appl. Mater. Interfaces* **2020**, *12*, 19184−19193.
(33) Joshi, P. B.; Karki, N.; Wilson, A. J. Electrocatalytic CO_2 Reduction in Acetonitrile Enhanced by the Local Environment and Mass Transport of H_2O. *ACS Energy Lett.* **2022**, *7*, 602−609.
(34) Liu, B.; Guo, W.; Gebbie, M. A. Tuning Ionic Screening To Accelerate Electrochemical CO_2 Reduction in Ionic Liquid Electrolytes. *ACS Catal.* **2022**, *12*, 9706−9716.
(35) Costentin, C.; Drouet, S.; Robert, M.; Savéant, J.-M. A local proton source enhances CO_2 electroreduction to CO by a molecular Fe catalyst. *Science* **2012**, *338*, 90−94.
(36) Wang, Y.; Hatakeyama, M.; Ogata, K.; Wakabayashi, M.; Jin, F.; Nakamura, S. Activation of CO_2 by ionic liquid EMIM−BF_4 in the electrochemical system: A theoretical study. *Phys. Chem. Chem. Phys.* **2015**, *17*, 23521−23531.
(37) Neyrizi, S.; Kiewiet, J.; Hempenius, M. A.; Mul, G. What It Takes for Imidazolium Cations to Promote Electrochemical Reduction of CO_2. *ACS Energy Lett.* **2022**, *7*, 3439−3446.
(38) Yim, J.-H.; Ha, S.-J.; Lim, J. S. Measurement and Correlation of CO_2 Solubility in 1-Ethyl-3-methylimidazolium ([EMIM]) Cation-Based Ionic Liquids: [EMIM][Ac], [EMIM][Cl], and [EMIM]-[$MeSO_4$]. *J. Chem. Eng. Data* **2018**, *63*, 508−518.
(39) Liu, H.; Huang, J.; Pendleton, P. Experimental and modelling study of CO_2 absorption in ionic liquids containing Zn (II) ions. *Energy Procedia* **2011**, *4*, 59−66.
(40) Sanchora, P.; Pandey, D. K.; Rana, D.; Materny, A.; Singh, D. K. Impact of Size and Electronegativity of Halide Anions on Hydrogen Bonds and Properties of 1-Ethyl-3-methylimidazolium-Based Ionic Liquids. *J. Phys. Chem. A* **2019**, *123*, 4948−4963.
(41) Dhumal, N. R.; Noack, K.; Kiefer, J.; Kim, H. J. Molecular Structure and Interactions in the Ionic Liquid 1-Ethyl-3-methylimidazolium Bis(Trifluoromethylsulfonyl)imide. *J. Phys. Chem. A* **2014**, *118*, 2547−2557.
(42) Socrates, G. *Infrared and Raman characteristic group frequencies: tables and charts, Chapter 13: Five-membered ring heterocyclic compounds*; John Wiley & Sons: 2004.
(43) Katayama, Y.; Nattino, F.; Giordano, L.; Hwang, J.; Rao, R. R.; Andreussi, O.; Marzari, N.; Shao-Horn, Y. An in situ surface-enhanced infrared absorption spectroscopy study of electrochemical CO_2 reduction: selectivity dependence on surface C-bound and O-bound reaction intermediates. *J. Phys. Chem. C* **2019**, *123*, 5951−5963.
(44) Jiang, S.; Klingan, K.; Pasquini, C.; Dau, H. New aspects of operando Raman spectroscopy applied to electrochemical CO_2 reduction on Cu foams. *J. Chem. Phys.* **2019**, *150*, No. 041718.
(45) Santos, V. O., Jr.; Leite, I. R.; Brolo, A. G.; Rubim, J. C. The electrochemical reduction of CO_2 on a copper electrode in 1-n-butyl-3-methyl imidazolium tetrafluoroborate ($BMI.BF_4$) monitored by surface-enhanced Raman scattering (SERS). *J. Raman Spectrosc.* **2016**, *47*, 674−680.
(46) Clark, M. L.; Ge, A.; Videla, P. E.; Rudshteyn, B.; Miller, C. J.; Song, J.; Batista, V. S.; Lian, T.; Kubiak, C. P. CO_2 Reduction Catalysts on Gold Electrode Surfaces Influenced by Large Electric Fields. *J. Am. Chem. Soc.* **2018**, *140*, 17643−17655.
(47) Min, Z.; Chang, B.; Shao, C.; Su, X.; Wang, N.; Li, Z.; Wang, H.; Zhao, Y.; Fan, M.; Wang, J. Enhancing CO2 electroreduction to syngas by active protons of imidazolium ionic liquids: From performance to mechanism. 2023, *326*, 122185, DOI: 10.1016/j.apcatb.2022.122185.
(48) Amyes, T. L.; Diver, S. T.; Richard, J. P.; Rivas, F. M.; Toth, K. Formation and stability of N-heterocyclic carbenes in water: the carbon acid pKa of imidazolium cations in aqueous solution. *J. Am. Chem. Soc.* **2004**, *126*, 4366−4374.
(49) Hangzhou LookChem Network Technology Co. Ltd. https://www.lookchem.com/ProductWholeProperty_LCPL279434.htm, (accessed March 20, 2023).
(50) Koshy, D. M.; Akhade, S. A.; Shugar, A.; Abiose, K.; Shi, J.; Liang, S.; Oakdale, J. S.; Weitzner, S. E.; Varley, J. B.; Duoss, E. B.; Baker, S. E.; Hahn, C.; Bao, Z.; Jaramillo, T. F. Chemical modifications of Ag catalyst surfaces with imidazolium ionomers modulate H_2 evolution rates during electrochemical CO_2 reduction. *J. Am. Chem. Soc.* **2021**, *143*, 14712−14725.